

# High-order finite volume WENO schemes for the shallow water equations with dry states

Yulong Xing<sup>1</sup> and Chi-Wang Shu<sup>2</sup>

## Abstract

The shallow water equations are used to model flows in rivers and coastal areas, and have wide applications in ocean, hydraulic engineering, and atmospheric modeling. These equations have still water steady state solutions in which the flux gradients are balanced by the source term. It is desirable to develop numerical methods which preserve exactly these steady state solutions. Another main difficulty usually arising from the simulation of dam breaks and flood waves flows is the appearance of dry areas where no water is present. If no special attention is paid, standard numerical methods may fail near dry/wet front and produce non-physical negative water height. A high-order accurate finite volume weighted essentially non-oscillatory (WENO) scheme is proposed in this paper to address these difficulties and to provide an efficient and robust method for solving the shallow water equations. A simple, easy-to-implement positivity-preserving limiter is introduced. One- and two-dimensional numerical examples are provided to verify the positivity-preserving property, well-balanced property, high-order accuracy, and good resolution for smooth and discontinuous solutions.

**Keywords:** shallow water equations; well-balanced; WENO scheme; finite volume method; positivity-preserving

---

<sup>1</sup>Computer Science and Mathematics Division, Oak Ridge National Laboratory, Oak Ridge, TN 37831 and Department of Mathematics, University of Tennessee, Knoxville, TN 37996. E-mail: xingy@math.utk.edu. Fax: (865) 574-0680. Research is sponsored by the Office of Advanced Scientific Computing Research; U.S. Department of Energy. The work was performed at the ORNL, which is managed by UT-Battelle, LLC under Contract No. DE-AC05-00OR22725.

<sup>2</sup>Division of Applied Mathematics, Brown University, Providence, RI 02912. E-mail: shu@dam.brown.edu. Research supported by DOE grant DE-FG02-08ER25863 and NSF grant DMS-0809086.

# 1 Introduction

The shallow water equations with a non-flat bottom topography play a critical role in the modeling and simulation of the flows in rivers and coastal areas, capturing fundamental phenomena across different length and time scales. They have wide applications in ocean and hydraulic engineering: tidal flows in estuary and coastal water region; bore wave propagation; and river, reservoir, and open channel flows, among others. If the non-flat bottom topography is considered, a source term will be added to the traditional shallow water equations, and they become a hyperbolic conservation law with a source term, also referred as a balance law. In one space dimension, the shallow water equations take the form

$$\begin{cases} h_t + (hu)_x = 0 \\ (hu)_t + \left(hu^2 + \frac{1}{2}gh^2\right)_x = -ghb_x, \end{cases} \quad (1.1)$$

where  $h$  denotes the water height,  $u$  is the velocity,  $b$  represents the bottom topography and  $g$  is the gravitational constant. In this paper, we will consider the variation of the bottom as the only source term, but other terms, such as friction term, could also be added.

An essential part for the shallow water equations and other balance laws is that they often admit steady state solutions in which the flux gradients are exactly balanced by the source term. The general steady state solutions of the shallow water equations (1.1) are given by

$$hu = \text{const} \quad \text{and} \quad \frac{1}{2}u^2 + g(h + b) = \text{const}, \quad (1.2)$$

and people are particularly interested in the still water at rest steady-state solution, which represents a still flat water surface:

$$u = 0 \quad \text{and} \quad h + b = \text{const}. \quad (1.3)$$

One main difficulty in solving (1.1) is the treatment of the source terms. Traditional numerical schemes without special handling of the source term, cannot balance the effect of the source term and the flux, and usually fail to capture the steady state well. They will introduce spurious oscillations near the steady state. In order to correctly resolve this steady

state, the grid must be extremely refined to reduce the size of these spurious oscillations, making the algorithm highly inefficient. The well-balanced schemes are developed to reduce the unnecessarily refined mesh for the shallow water simulation. They are specially designed to preserve exactly these steady-state solutions up to machine error with relatively coarse meshes. Research on well-balanced numerical methods for the shallow water system has attracted tremendous attention in the past two decades. Many researchers have developed well-balanced methods for the shallow water equations using different approaches, see, e.g. [3, 1, 24, 2, 30, 22, 17] and the references therein.

Another difficulty often encountered in the simulations of the shallow water equations is the appearance of dry areas where no water is present. Typical applications include the dam break problem, flood waves and run-up phenomena at a coast with tsunamis being the most impressive example. The difficulty in numerically modeling these dry areas relates to the fact that there is no water in these areas, while the shallow water equations (1.1) are only defined in wet regions. Therefore we need to deal with moving boundary problems for the shallow water equations. There are many existing wetting and drying treatments using different approaches in the literature. The first type is the mesh adaption technique [5] which tracks the dry front by changing the meshes. It has the advantage in accuracy but is computationally expensive. The second type [15] uses the mesh reduction technique with fixed meshes, which removes the dry elements and restores them when they become wet later. It may cause oscillations and a loss of mass and momentum (failure in conservation). A more popular approach is the thin layer technique [8, 7, 13, 25, 23, 6], which maintains a very thin layer in dry elements and includes these dry elements in the computation. Special attention need to be paid near the dry/wet front, otherwise they may produce non-physical negative water height, which becomes problematic when calculating the eigenvalues  $u \pm \sqrt{gh}$  to determine the time step size  $\Delta t$ , and renders the system not hyperbolic and not well posed.

In recent years, high-order accurate numerical schemes (with higher than second-order

accuracy), have attracted increasing attention in many computational fields. They have been developed to reduce the number of computational cells and minimize the computational time to achieve the desired resolution. Examples include finite difference/volume weighted essentially non-oscillatory (WENO) schemes, spectral methods and discontinuous Galerkin (DG) methods. They have been applied to solve the shallow water equations [26, 16, 14, 20] and achieved good results. However, it would be desirable to develop high-order methods for the shallow water equations, which could also overcome the two above-mentioned difficulties. In this direction, several high-order well-balanced methods have been proposed, by Xing and Shu [36, 37, 38], Noelle et al. [27], Pares et al. [12, 28] and other researchers [10, 9, 11]. Discussions on high-order methods involving wetting and drying treatments for the shallow water equations include [4, 15, 18]. Most existing wetting and drying treatments are focused on post-processing reconstruction of the data obtained from the numerical solution at each time level. One example is to project the solution to a non-negative linear element in the cell near the wet/dry front. Even though the post-processing can bring the reconstruction to satisfy non-negative water height, this alone usually does *not* guarantee that the solution (e.g., cell average from a finite volume or DG scheme) at the next time step still maintains the non-negative water height property. If negative cell averages for the water height are obtained at the next time level, the positivity reconstruction post-processing will destroy the conservation.

The main objective of this paper is to develop high-order mass-conserving finite volume WENO methods for the shallow water equations with dry areas. The proposed methods are genuinely high-order, well-balanced for the still water solution and preserve the non-negativity of the water height without loss of mass conservation. A maximum-principle-satisfying limiter was proposed by one of the authors and his collaborators in [29, 40, 41]. The generalization of this limiter to the shallow water equations in the DG formulation has been studied in [39] to develop positivity-preserving well-balanced DG methods. In this paper, we will address the finite volume generalization of this limiter to the shallow water

equations and couple this limiter with well-balanced methods. Note that the maximum-principle finite volume limiter introduced in [40] for the scalar equation involves extra WENO reconstructions to compute the values at the quadrature points. These lead to additional computational costs, rendering the algorithm less efficient for 2D problems. In the present work we use a slightly modified version of this limiter, see also [42], which does not require these extra WENO reconstructions and is very efficient to implement. The resulting limiter shares the same property as the original one, and will be carefully coupled with the well-balanced techniques for the shallow water equations. The well-balanced positivity-preserving method is first introduced in one dimension and then extended to two dimensions with rectangular meshes.

This paper is organized as follows. In Section 2, we give a brief review of the well-balanced finite volume WENO methods for the shallow water equations proposed in [38]. In Section 3, we first present a positivity-preserving limiter, which keeps the water height non-negative, preserves the mass conservation and at the same time does not affect the high-order accuracy for the general solutions. The well-balanced positivity-preserving WENO method with wetting and drying treatment is then developed and its algorithm flowchart is also provided. Extension to two dimensions with rectangular meshes is introduced in Section 4. Section 5 contains extensive numerical results to demonstrate the behavior of the proposed finite volume WENO methods for one- and two-dimensional shallow water equations. Concluding remarks are given in Section 6.

## 2 Well-balanced finite volume WENO methods

Finite volume schemes are very popular for solving hyperbolic conservation laws. They represent the underlying physics in a natural way. In this section, we recall the high-order well-balanced finite volume WENO schemes developed by the authors in [38]. Only the one-dimensional approach will be briefly reviewed, and we refer to [38] for further details. This method will serve as the starting point for our extensions to the shallow water equations

with dry areas.

We discretize the computational domain into cells  $I_j = [x_{j-\frac{1}{2}}, x_{j+\frac{1}{2}}]$ , and denote the size of the  $j$ -th cell by  $\Delta x_j$  and the maximum mesh size by  $\Delta x = \max_j \Delta x_j$ . For the ease of presentation, we denote the shallow water equations (1.1) by

$$U_t + f(U)_x = s(h, b)$$

where  $U = (h, hu)^T$  with the superscript  $T$  denoting the transpose,  $f(U)$  is the flux and  $s(h, b)$  is the source term. In a finite volume scheme, our computational variables are  $\bar{U}_j(t)$ , which approximate the cell averages  $\bar{U}(x_j, t) = \frac{1}{\Delta x_j} \int_{I_j} U(x, t) dx$ . The conservative numerical scheme is given by

$$\frac{d}{dt} \bar{U}_j(t) + \frac{1}{\Delta x_j} \left( \hat{f}_{j+\frac{1}{2}} - \hat{f}_{j-\frac{1}{2}} \right) = \frac{1}{\Delta x_j} \int_{I_j} s(h, b) dx, \quad (2.1)$$

with  $\hat{f}_{j+\frac{1}{2}} = F(U_{j+\frac{1}{2}}^-, U_{j+\frac{1}{2}}^+)$  being the numerical flux. The simplest and most inexpensive numerical flux is the Lax-Friedrichs flux

$$F(a, b) = \frac{1}{2}(f(a) + f(b) - \alpha(b - a)), \quad (2.2)$$

where  $\alpha = \max(|u| + \sqrt{gh})$  and the maximum is taken over the whole domain.  $U_{j+\frac{1}{2}}^-$  and  $U_{j+\frac{1}{2}}^+$ , the high-order pointwise approximations to  $U(x_{j+\frac{1}{2}}, t)$  from left and right respectively, are computed through the neighboring cell average values  $\bar{U}_j$  by a high order WENO reconstruction procedure. Basically, for a  $(2k - 1)$ -th order WENO scheme, we first compute  $k$  reconstructed boundary values  $U_{j+\frac{1}{2}}^{(k), \pm}$  corresponding to different candidate stencils. Then by providing each value a weight which indicates the smoothness of the corresponding stencil, we define the  $(2k - 1)$ -th order WENO reconstruction  $U_{j+\frac{1}{2}}^\pm$  as a convex combination of all these  $k$  reconstructed values. Eventually, the WENO reconstruction can be written out as:

$$U_{j+\frac{1}{2}}^+ = \sum_{r=-k+1}^k w_r \bar{U}_{j+r}, \quad U_{j+\frac{1}{2}}^- = \sum_{r=-k}^{k-1} \tilde{w}_r \bar{U}_{j+r}. \quad (2.3)$$

where  $k = 3$  for the fifth order WENO approximation and the coefficients  $w_r$  and  $\tilde{w}_r$  depend nonlinearly on the smoothness indicators involving the cell average  $\bar{u}$  and satisfy

$\sum_{r=-k+1}^k w_r = \sum_{r=-k}^{k-1} \tilde{w}_r = 1$ . For hyperbolic systems, we usually use the local characteristic decomposition, which is more robust than a component by component version. The complete algorithm can be found in [21, 32, 34].

Total variation diminishing (TVD) high-order Runge-Kutta time discretization [35] is used in practice for stability and to increase temporal accuracy. For example, the third order TVD Runge-Kutta method is used in the simulation in this paper:

$$\begin{aligned} U^{(1)} &= U^n + \Delta t \mathcal{F}(U^n) \\ U^{(2)} &= \frac{3}{4}U^n + \frac{1}{4}(U^{(1)} + \Delta t \mathcal{F}(U^{(1)})) \\ U^{n+1} &= \frac{1}{3}U^n + \frac{2}{3}(U^{(2)} + \Delta t \mathcal{F}(U^{(2)})), \end{aligned} \quad (2.4)$$

where  $\mathcal{F}(U)$  is the spatial operator.

In order to achieve the well-balanced property, we are interested in preserving the still water stationary solution (1.3) exactly. As mentioned in [38], our well-balanced numerical scheme, with a simple Euler forward time discretization, has the form

$$\frac{U^{n+1} - U^n}{\Delta t} + \frac{1}{\Delta x_j} (\hat{f}_{j+\frac{1}{2}}^l - \hat{f}_{j-\frac{1}{2}}^r) = \frac{1}{\Delta x_j} \int_{I_j} s(h^n, b) dx. \quad (2.5)$$

The left and right fluxes  $\hat{f}_{j+\frac{1}{2}}^l$  and  $\hat{f}_{j-\frac{1}{2}}^r$  are given by:

$$\begin{aligned} \hat{f}_{j+\frac{1}{2}}^l &= F(U_{j+\frac{1}{2}}^{*, -}, U_{j+\frac{1}{2}}^{*, +}) + \begin{pmatrix} 0 \\ \frac{g}{2}(h_{j+\frac{1}{2}}^-)^2 - \frac{g}{2}(h_{j+\frac{1}{2}}^{*, -})^2 \end{pmatrix} \\ \hat{f}_{j-\frac{1}{2}}^r &= F(U_{j-\frac{1}{2}}^{*, -}, U_{j-\frac{1}{2}}^{*, +}) + \begin{pmatrix} 0 \\ \frac{g}{2}(h_{j-\frac{1}{2}}^+)^2 - \frac{g}{2}(h_{j-\frac{1}{2}}^{*, +})^2 \end{pmatrix}. \end{aligned} \quad (2.6)$$

with the left and right values of  $U^*$  defined as:

$$U_{j+\frac{1}{2}}^{*, \pm} = \begin{pmatrix} h_{j+\frac{1}{2}}^{*, \pm} \\ h_{j+\frac{1}{2}}^{*, \pm} u_{j+\frac{1}{2}}^{\pm} \end{pmatrix}, \quad (2.7)$$

$$h_{j+\frac{1}{2}}^{*, \pm} = \max \left( 0, h_{j+\frac{1}{2}}^{\pm} + b_{j+\frac{1}{2}}^{\pm} - \max(b_{j+\frac{1}{2}}^+, b_{j+\frac{1}{2}}^-) \right). \quad (2.8)$$

To compute the well-balanced approximation of the source term, we first construct  $b_{j+\frac{1}{2}}^{\pm}$ , which should satisfy that  $h_{j+\frac{1}{2}}^{\pm} + b_{j+\frac{1}{2}}^{\pm} = \text{const}$  if the still water  $\bar{h}_j + \bar{b}_j = \text{const}$  is given. It

can be achieved by applying the same coefficients  $w_r$  and  $\tilde{w}_r$  used in (2.3) on  $B = (b, 0)^T$  to obtain

$$B_{j+\frac{1}{2}}^+ = \sum_{r=-k+1}^k w_r \bar{B}_{j+r}, \quad B_{j+\frac{1}{2}}^- = \sum_{r=-k}^{k-1} \tilde{w}_r \bar{B}_{j+r}. \quad (2.9)$$

Note that these coefficients  $w_r$  and  $\tilde{w}_r$  depend nonlinearly on the variables  $\bar{U}_j$ . Hence,

$$U_{j+\frac{1}{2}}^+ + B_{j+\frac{1}{2}}^+ = \sum_{r=-k+1}^k w_r (\bar{U}_{j+r} + \bar{B}_{j+r}), \quad U_{j+\frac{1}{2}}^- + B_{j+\frac{1}{2}}^- = \sum_{r=-k}^{k-1} \tilde{w}_r (\bar{U}_{j+r} + \bar{B}_{j+r}),$$

from which we know that the reconstructed values satisfy  $h_{j+\frac{1}{2}}^\pm + b_{j+\frac{1}{2}}^\pm = \text{const}$  for still water. Then, we use interpolation to obtain a high-order polynomial  $h_h$  (or  $b_h$ ) on the cell  $I_j$ , based on the boundary values  $h_{j-\frac{1}{2}}^+, h_{j+\frac{1}{2}}^-$  (or  $b_{j-\frac{1}{2}}^+, b_{j+\frac{1}{2}}^-$ ) and several other neighboring boundary values. For example, we can use  $h_{j+\frac{3}{2}}^-, h_{j+\frac{1}{2}}^-, h_{j-\frac{1}{2}}^+$  and  $h_{j-\frac{3}{2}}^+$  to interpolate a third degree polynomial. Therefore,  $\int_{I_j} s(h_h, b_h) dx$ , a high-order approximation to the source term  $\int_{I_j} s(h, b) dx$ , can be exactly computed by a suitable Gauss quadrature. In order to obtain  $(2k-1)$ -th order accurate method,  $h_h$  and  $b_h$  need to approximate  $h$  and  $b$  with  $(k+1)$ -th order accuracy. Combining these together, we have proven in [38] that the above methods (2.5) are actually well-balanced for the still water steady state (1.3) of the shallow water equations.

### 3 Positivity-preserving high-order WENO methods

In this section, we first present a positivity-preserving limiter for the shallow water equations (1.1) with dry areas, to guarantee that no negative water height will be generated during the computing, even near the wet/dry front. We consider the Euler forward in time (2.5) first. Higher order time discretization will be discussed later in this section.

By plugging (2.7) and (2.6) into (2.5), the scheme satisfied by the cell averages of the water height in the well-balanced finite volume WENO methods (2.5) can be written as

$$\bar{h}_j^{n+1} = \bar{h}_j^n - \lambda \left[ \widehat{F} \left( h_{j+\frac{1}{2}}^{*-}, u_{j+\frac{1}{2}}^-; h_{j+\frac{1}{2}}^{*+}, u_{j+\frac{1}{2}}^+ \right) - \widehat{F} \left( h_{j-\frac{1}{2}}^{*-}, u_{j-\frac{1}{2}}^-; h_{j-\frac{1}{2}}^{*+}, u_{j-\frac{1}{2}}^+ \right) \right], \quad (3.1)$$

where  $\lambda = \Delta x / \Delta t$ ,  $h_{j+\frac{1}{2}}^{*,\pm}$  are defined in (2.8) and

$$\widehat{F} \left( h_{j+\frac{1}{2}}^{*,-}, u_{j+\frac{1}{2}}^-; h_{j+\frac{1}{2}}^{*,+}, u_{j+\frac{1}{2}}^+ \right) = \frac{1}{2} \left( h_{j+\frac{1}{2}}^{*,-} u_{j+\frac{1}{2}}^- + h_{j+\frac{1}{2}}^{*,+} u_{j+\frac{1}{2}}^+ - \alpha (h_{j+\frac{1}{2}}^{*,+} - h_{j+\frac{1}{2}}^{*,-}) \right). \quad (3.2)$$

We start by showing the following lemma on the positivity of a first order scheme with the well-balanced flux, and refer to [39] for the detailed proof.

**Lemma 3.1:** Under the CFL condition  $\lambda\alpha \leq 1$ , with  $\alpha = \max(|u| + \sqrt{gh})$ , consider the following scheme

$$h_j^{n+1} = h_j^n - \lambda \left[ \widehat{F} \left( h_j^{*,+}, u_j^n; h_{j+1}^{*,-}, u_{j+1}^n \right) - \widehat{F} \left( h_{j-1}^{*,+}, u_{j-1}^n; h_j^{*,-}, u_j^n \right) \right] \quad (3.3)$$

with  $\widehat{F}$  the same as in (3.2) and

$$\begin{aligned} h_j^{*,+} &= \max \left( 0, h_j^n + b_j - \max(b_j, b_{j+1}) \right) \\ h_j^{*,-} &= \max \left( 0, h_j^n + b_j - \max(b_{j-1}, b_j) \right). \end{aligned}$$

If  $h_j^n, h_{j\pm 1}^n$  are non-negative, then  $h_j^{n+1}$  is also non-negative.

We now consider the  $(2k - 1)$ -th order scheme (3.1). For the ease of presentation, we consider a reconstructed polynomial  $p_j(x)$  of degree  $2k - 2$ , which satisfies

$$p_j(x_{j-\frac{1}{2}}) = h_{j-\frac{1}{2}}^+, \quad p_j(x_{j+\frac{1}{2}}) = h_{j+\frac{1}{2}}^-, \quad \frac{1}{\Delta x} \int_{I_j} p_j(x) dx = \overline{h}_j^n. \quad (3.4)$$

Moreover,  $p_j(x)$  should be a  $(2k - 1)$ -th order accurate approximation to the exact solution on  $I_j$ . As we will explain later, this polynomial only serves the theoretical purpose to understand the derivation of the limiter and will not need to be explicitly constructed in the implementation.

Let us introduce the  $N$ -point Legendre Gauss-Lobatto quadrature rule on the interval  $I_j = [x_{j-\frac{1}{2}}, x_{j+\frac{1}{2}}]$ , which is exact for the integral of polynomials of degree up to  $2N - 3$ .  $N$  is chosen such that  $2N - 3 \geq 2k - 2$ . We denote these quadrature points on  $I_j$  as

$$S_j = \left\{ x_{j-\frac{1}{2}} = \widehat{x}_j^1, \widehat{x}_j^2, \dots, \widehat{x}_j^{N-1}, \widehat{x}_j^N = x_{j+\frac{1}{2}} \right\}.$$

Let  $\hat{w}_r$  be the quadrature weights for the interval  $[-1/2, 1/2]$  such that  $\sum_{r=1}^N \hat{w}_r = 1$ . Since the quadrature is exact for polynomials of degree  $2k - 2$ , we have

$$\bar{h}_j^n = \frac{1}{\Delta x} \int_{I_j} p_j(x) dx = \sum_{r=1}^N \hat{w}_r p_j(\hat{x}_j^r) = \sum_{r=2}^{N-1} \hat{w}_r p_j(\hat{x}_j^r) + \hat{w}_1 h_{j-\frac{1}{2}}^+ + \hat{w}_N h_{j+\frac{1}{2}}^-. \quad (3.5)$$

If we introduce the variable

$$\xi_j = \frac{1}{\sum_{r=2}^{N-1} \hat{w}_r} \sum_{t=2}^{N-1} \hat{w}_t p_j(\hat{x}_j^t) = \frac{\bar{h}_j^n - \hat{w}_1 h_{j-\frac{1}{2}}^+ - \hat{w}_N h_{j+\frac{1}{2}}^-}{1 - \hat{w}_1 - \hat{w}_N}, \quad (3.6)$$

we have

$$\bar{h}_j^n = (1 - \hat{w}_1 - \hat{w}_N) \xi_j + \hat{w}_1 h_{j-\frac{1}{2}}^+ + \hat{w}_N h_{j+\frac{1}{2}}^-. \quad (3.7)$$

Following the approaches in [29], [40] and [39], we have the following result.

**Proposition 3.2:** Consider the scheme (3.1) satisfied by the cell averages of the water height. Let  $\xi_j$  be defined in (3.6). If  $h_{j-\frac{1}{2}}^\pm$ ,  $h_{j+\frac{1}{2}}^\pm$  and  $\xi_j$  are all non-negative, then  $\bar{h}_j^{n+1}$  is also non-negative under the CFL condition

$$\lambda \alpha \leq \hat{w}_1. \quad (3.8)$$

**Proof:** Plug (3.7) into (3.1) and rewrite (3.1) by adding and subtracting the term

$$\widehat{F} \left( h_{j-\frac{1}{2}}^{*,+}, u_{j-\frac{1}{2}}^+; h_{j+\frac{1}{2}}^{*,-}, u_{j+\frac{1}{2}}^- \right):$$

$$\begin{aligned} \bar{h}_j^{n+1} &= (1 - \hat{w}_1 - \hat{w}_N) \xi_j + \hat{w}_1 h_{j-\frac{1}{2}}^+ + \hat{w}_N h_{j+\frac{1}{2}}^- \\ &\quad - \lambda \left[ \widehat{F} \left( h_{j+\frac{1}{2}}^{*,-}, u_{j+\frac{1}{2}}^-; h_{j+\frac{1}{2}}^{*,+}, u_{j+\frac{1}{2}}^+ \right) - \widehat{F} \left( h_{j-\frac{1}{2}}^{*,+}, u_{j-\frac{1}{2}}^+; h_{j+\frac{1}{2}}^{*,-}, u_{j+\frac{1}{2}}^- \right) \right. \\ &\quad \left. + \widehat{F} \left( h_{j-\frac{1}{2}}^{*,+}, u_{j-\frac{1}{2}}^+; h_{j+\frac{1}{2}}^{*,-}, u_{j+\frac{1}{2}}^- \right) - \widehat{F} \left( h_{j-\frac{1}{2}}^{*,-}, u_{j-\frac{1}{2}}^-; h_{j-\frac{1}{2}}^{*,+}, u_{j-\frac{1}{2}}^+ \right) \right] \\ &= (1 - \hat{w}_1 - \hat{w}_N) \xi_j + \hat{w}_N H_N + \hat{w}_1 H_1, \end{aligned}$$

where

$$H_1 = h_{j-\frac{1}{2}}^+ - \frac{\lambda}{\hat{w}_1} \left[ \widehat{F} \left( h_{j-\frac{1}{2}}^{*,+}, u_{j-\frac{1}{2}}^+; h_{j+\frac{1}{2}}^{*,-}, u_{j+\frac{1}{2}}^- \right) - \widehat{F} \left( h_{j-\frac{1}{2}}^{*,-}, u_{j-\frac{1}{2}}^-; h_{j-\frac{1}{2}}^{*,+}, u_{j-\frac{1}{2}}^+ \right) \right], \quad (3.9)$$

$$H_N = h_{j+\frac{1}{2}}^- - \frac{\lambda}{\hat{w}_N} \left[ \widehat{F} \left( h_{j+\frac{1}{2}}^{*,-}, u_{j+\frac{1}{2}}^-; h_{j+\frac{1}{2}}^{*,+}, u_{j+\frac{1}{2}}^+ \right) - \widehat{F} \left( h_{j-\frac{1}{2}}^{*,+}, u_{j-\frac{1}{2}}^+; h_{j+\frac{1}{2}}^{*,-}, u_{j+\frac{1}{2}}^- \right) \right]. \quad (3.10)$$

Notice that (3.9) and (3.10) are both of the type (3.3), hence  $H_1 \geq 0$  and  $H_N \geq 0$  under the suitable CFL conditions, which are  $\frac{\lambda}{\hat{w}_1}\alpha \leq 1$  and  $\frac{\lambda}{\hat{w}_N}\alpha \leq 1$  respectively. Since  $\hat{w}_1 = \hat{w}_N$ , these two CFL conditions are the same and become (3.8). Therefore  $\bar{h}_j^{n+1} \geq 0$ , since it is a convex combination of  $H_1$ ,  $H_N$  and  $\xi_j$ .  $\square$

This proposition tells us that for the scheme (3.1), we need to modify  $p_j(x)$  (satisfying (3.4)) such that  $p_j(x_{j\pm\frac{1}{2}})$  and  $\xi_j$  are all non-negative. At time level  $n$ , given  $\bar{h}_j^n \geq 0$ , we consider the following limiter on the piecewise polynomial  $p_j(x)$  introduced in [40]. It is a linear scaling around the cell average:

$$\tilde{p}_j(x) = \theta \left( p_j(x) - \bar{h}_j^n \right) + \bar{h}_j^n, \quad \theta = \min \left\{ 1, \frac{\bar{h}_j^n}{\bar{h}_j^n - m_j} \right\}, \quad (3.11)$$

with

$$m_j = \min_{x \in I_j} p_j(x). \quad (3.12)$$

It is easy to observe that the conditions of Proposition 3.2 are satisfied after this limiter. Moreover, it can also be shown that this limiter does not destroy the high-order accuracy, and we refer to [40] for the detailed proof. Let  $\tilde{h}_{j-\frac{1}{2}}^+ = \tilde{p}_j(x_{j-\frac{1}{2}})$ ,  $\tilde{h}_{j+\frac{1}{2}}^- = \tilde{p}_j(x_{j+\frac{1}{2}})$ , and define  $\tilde{h}_{j-\frac{1}{2}}^{*,+}$ ,  $\tilde{h}_{j+\frac{1}{2}}^{*,-}$  following (2.8). Then, the revised positivity-preserving version of the scheme (3.1) takes the form

$$\bar{h}_j^{n+1} = \bar{h}_j^n - \lambda \left[ \widehat{F} \left( \tilde{h}_{j+\frac{1}{2}}^{*,-}, u_{j+\frac{1}{2}}^-; \tilde{h}_{j+\frac{1}{2}}^{*,+}, u_{j+\frac{1}{2}}^+ \right) - \widehat{F} \left( \tilde{h}_{j-\frac{1}{2}}^{*,-}, u_{j-\frac{1}{2}}^-; \tilde{h}_{j-\frac{1}{2}}^{*,+}, u_{j-\frac{1}{2}}^+ \right) \right]. \quad (3.13)$$

Notice that in (3.12) we need to evaluate the minimum of a polynomial. We prefer to avoid evaluating the extrema of a polynomial, especially since we will extend the method to two dimensions. In [40] and [39], (3.12) was replaced by

$$m_j = \min_{x \in S_j} p_j(x) = \min_{t=1, \dots, N} p_j(\hat{x}_j^t), \quad (3.14)$$

which involves the computation of the values of a polynomial at these Gauss quadrature points. For the finite volume WENO schemes, an extra Hermite type reconstruction was introduced in [40] to compute them. This step becomes rather complicated and time-consuming for two-dimensional problems, as shown in [40].

In this paper, we use a simpler approach, see also [42], which does not require an explicit construction of this additional reconstruction polynomial. The additional computational cost for the positivity-preserving limiter (3.11) is therefore negligible. The idea is to replace (3.12) by

$$m_j = \min(h_{j-\frac{1}{2}}^+, h_{j+\frac{1}{2}}^-, \xi_j). \quad (3.15)$$

Since  $\xi_j$  can be computed by (3.6) easily, it is very easy to evaluate  $m_j$ . We will show in the next lemma that the approach (3.15) inherits the desirable properties of (3.12).

**Lemma 3.3:** Assume  $\bar{h}_j^n \geq 0$ , then the limiter (3.11) and (3.15) is a high-order accurate positivity-preserving limiter, and preserves the conservation of  $p_j(x)$ .

**Proof:** It is easy to observe that this limiter preserves the local conservation since  $\int_{I_j} \tilde{p}_j(x) dx = \int_{I_j} p_j(x) dx$ . Next, we would like to show that after the limiter (3.11) and (3.15),  $\tilde{h}_{j-\frac{1}{2}}^+$ ,  $\tilde{h}_{j+\frac{1}{2}}^-$  and  $\tilde{\xi}_j$  are all non-negative, then the conditions of Proposition 3.2 are valid. The first two are trivial to show, and we look closely at  $\tilde{\xi}_j$ .

It is easy to derive that

$$\begin{aligned} \tilde{\xi}_j &= \frac{1}{\sum_{t=2}^{N-1} \hat{w}_t} \sum_{t=2}^{N-1} \hat{w}_t \tilde{p}_j(\hat{x}_j^t) = \theta \left( \frac{1}{\sum_{t=2}^{N-1} \hat{w}_t} \sum_{t=2}^{N-1} \hat{w}_t p_j(\hat{x}_j^t) - \bar{h}_j^n \right) + \bar{h}_j^n \\ &= \theta (\xi_j - \bar{h}_j^n) + \bar{h}_j^n = \theta \xi_j + (1 - \theta) \bar{h}_j^n. \end{aligned}$$

If  $\xi_j \geq 0$ , we also have  $\tilde{\xi}_j \geq 0$ . If  $\xi_j < 0$ , we know  $m_j = \min(h_{j-\frac{1}{2}}^+, h_{j+\frac{1}{2}}^-, \xi_j) \leq \xi_j < 0 \leq \bar{h}_j^n$ , and

$$\theta = \frac{\bar{h}_j^n}{\bar{h}_j^n - m_j} \leq \frac{\bar{h}_j^n}{\bar{h}_j^n - \xi_j}.$$

Therefore,

$$\tilde{\xi}_j = \theta (\xi_j - \bar{h}_j^n) + \bar{h}_j^n \geq \frac{\bar{h}_j^n}{\bar{h}_j^n - \xi_j} (\xi_j - \bar{h}_j^n) + \bar{h}_j^n = -\bar{h}_j^n + \bar{h}_j^n = 0.$$

In the end, we prove the high-order accuracy of this limiter (3.11) and (3.15). During the proof, we would like to use the conclusion that the limiter (3.11) and (3.14) is high-order

accurate (see [40] for a proof). We denoted the output of that limiter as  $\hat{p}_j(x)$ , and have  $\hat{p}_j(x) - p_j(x) = O(\Delta x^{2k-1})$ . Since  $\xi_j \geq \min_{t=2, \dots, N-1} p_j(\hat{x}_j^t)$ , we have

$$m_j = \min(h_{j-\frac{1}{2}}^+, h_{j+\frac{1}{2}}^-, \xi_j) \geq \min_{t=1, \dots, N} p_j(\hat{x}_j^t),$$

or equivalently

$$\theta = \min \left\{ 1, \left| \frac{\bar{h}_j^n}{\bar{h}_j^n - m_j} \right| \right\} \geq \min \left\{ 1, \left| \frac{\bar{h}_j^n}{\bar{h}_j^n - \min_{t=1, \dots, N} p_j(\hat{x}_j^t)} \right| \right\} \equiv \hat{\theta}$$

Therefore,

$$\begin{aligned} |\tilde{p}_j(x) - p_j(x)| &= (1 - \theta) |p_j(x) - \bar{h}_j^n| \\ &\leq (1 - \hat{\theta}) |p_j(x) - \bar{h}_j^n| = |\hat{p}_j(x) - p_j(x)| = O(\Delta x^{2k-1}), \end{aligned}$$

and we can conclude that  $\tilde{p}_j(x)$  is also a high-order accurate approximation to  $p_j(x)$ .  $\square$

We would like to mention that in wet region, where  $m_j$  is  $O(1)$  above zero, the limiter does not take any effect, i.e.,  $\tilde{p}_j(x) = p_j(x)$ . Therefore this positivity-preserving limiter is active only in the dry or nearly dry region. We now have the following proposition.

**Proposition 3.4:** Consider the revised numerical scheme (3.13), with the positivity-preserving limiter (3.11), (3.15), i.e.

$$\tilde{h}_{j-\frac{1}{2}}^+ = \theta \left( h_{j-\frac{1}{2}}^+ - \bar{h}_j^n \right) + \bar{h}_j^n, \quad \tilde{h}_{j+\frac{1}{2}}^- = \theta \left( h_{j+\frac{1}{2}}^- - \bar{h}_j^n \right) + \bar{h}_j^n, \quad (3.16)$$

with  $\theta$  computed in (3.15). Suppose the well-balanced flux (2.7) is used, with  $\tilde{h}_{j-\frac{1}{2}}^{*,+}$ ,  $\tilde{h}_{j+\frac{1}{2}}^{*,-}$  computed following (2.8). This method is  $(2k - 1)$ -th order accurate, positivity-preserving and conserves the mass conservation, under the CFL condition (3.8). For a fifth-order WENO scheme with  $k = 3$ , this CFL condition is  $\lambda\alpha \leq 1/12$ .

**Remark 3.5:** Here we only discuss the Euler forward time discretization. TVD high-order Runge-Kutta [35] and multi-step [33] time discretizations will keep the validity of the

proposition since TVD time discretizations are convex combinations of the Euler forward operators.

**Remark 3.6:** The Gauss-Lobatto quadrature only serves the purpose towards the proof of the Proposition 3.2 and 3.4. We do not use this quadrature explicitly during the computing. The only thing that is related with this quadrature is the CFL condition (3.8) which depends on  $\hat{w}_1$ . Especially, note that it has nothing to do with the computation of the cell integrals in (2.5), for which we can use any quadrature as long as the accuracy requirement is satisfied.

**Remark 3.7:** Note that although the well-balanced flux (2.6) is used throughout the proof, the result also holds for the traditional WENO methods using the flux (2.2) without the correction (2.6). Any other positivity-preserving exact or approximate Riemann solver, including Godunov, Boltzmann type and Harten-Lax-Van Leer, will also work under the corresponding CFL condition. Also, although the equation for the positivity variable  $h$  does not have a source term, we would like to comment that combining the well-balanced scheme with the positivity-preserving limiter is still non-trivial. For example, the well-balanced WENO method developed in [37] cannot be extended in the same fashion.

Given the cell average  $\bar{U}_j^n$  in interval  $I_j$  at time level  $n$  with a non-negative height cell average  $\bar{h}_j^n \geq 0$ , the algorithm flowchart of our high-order well-balanced positivity-preserving WENO method with Euler forward in time for the shallow water equations is:

- Use WENO reconstruction to evaluate  $U_{j-\frac{1}{2}}^+$  and  $U_{j+\frac{1}{2}}^-$ , and compute  $\xi_j$  from (3.6).
- Evaluate  $m_j$  by (3.15) and use the positivity preserving limiter (3.16) to compute  $\tilde{h}_{j-\frac{1}{2}}^+$  and  $\tilde{h}_{j+\frac{1}{2}}^-$ .
- Compute  $\tilde{U}_{j-\frac{1}{2}}^{*,+}$  and  $\tilde{U}_{j+\frac{1}{2}}^{*,-}$  following (2.8) and use them instead of  $U_{j-\frac{1}{2}}^{*,+}$ ,  $U_{j+\frac{1}{2}}^{*,-}$  in the WENO scheme (2.5) with the CFL condition (3.8).

For TVD high-order time discretizations, we need to perform the algorithm above in each stage for a Runge-Kutta method or in each step for a multistep method.

## 4 Two-dimensional extension

In this section, we construct the positivity-preserving well-balanced WENO scheme on rectangular meshes to solve the two-dimensional shallow water equations:

$$\begin{cases} h_t + (hu)_x + (hv)_y = 0 \\ (hu)_t + \left(hu^2 + \frac{1}{2}gh^2\right)_x + (huv)_y = -ghb_x \\ (hv)_t + (huv)_x + \left(hv^2 + \frac{1}{2}gh^2\right)_y = -ghb_y, \end{cases} \quad (4.1)$$

where  $(u, v)$  is the velocity of the fluid, and  $h, b$  and  $g$  follow the definitions below (1.1). For the ease of presentation, we denote this equation (4.1) by

$$U_t + f(U)_x + g(U)_y = s(h, b)$$

where  $U = (h, hu, hv)^T$ , and  $f(U), g(U)$  are the fluxes. The still water stationary solution we are interested to preserve is

$$h + b = \text{const}, \quad hu = 0, \quad hv = 0. \quad (4.2)$$

We discretize the computational domain into cells  $I_{i,j} = [x_{i-\frac{1}{2}}, x_{i+\frac{1}{2}}] \times [y_{j-\frac{1}{2}}, y_{j+\frac{1}{2}}]$ . For simplicity, we assume a uniform mesh is used. The sizes of each rectangle cell are denoted by  $\Delta x$  and  $\Delta y$ , with  $\lambda_1 = \Delta t/\Delta x$ ,  $\lambda_2 = \Delta t/\Delta y$ . The integrals will be approximated by quadratures with sufficient accuracy. Let us assume that we use a Gauss quadrature with  $L$  points, which is exact for single variable polynomials of degree  $2k - 2$ . We assume

$$S_i^x = \{x_i^\beta : \beta = 1, \dots, L\}, \quad S_j^y = \{y_j^\beta : \beta = 1, \dots, L\} \quad (4.3)$$

denote the Gauss quadrature points on  $[x_{i-\frac{1}{2}}, x_{i+\frac{1}{2}}]$  and  $[y_{j-\frac{1}{2}}, y_{j+\frac{1}{2}}]$ , respectively. For instance,  $(x_{i-\frac{1}{2}}^\beta, y_j^\beta)$  ( $\beta = 1, \dots, L$ ) are the Gauss quadrature points on the left edge of the  $(i, j)$  cell. Let  $w_\beta$  be the Gaussian quadrature weights for the interval  $[-\frac{1}{2}, \frac{1}{2}]$ .

We only discuss Euler forward in time for the same reason as in Section 3. The two-dimensional WENO method is given by

$$\frac{U^{n+1} - U^n}{\Delta t} = -\frac{1}{\Delta x} \left( \widehat{f}_{i+\frac{1}{2},j} - \widehat{f}_{i-\frac{1}{2},j} \right) - \frac{1}{\Delta y} \left( \widehat{g}_{i,j+\frac{1}{2}} - \widehat{g}_{i,j-\frac{1}{2}} \right) + \frac{1}{\Delta x \Delta y} \int_{I_{i,j}} s(h, b) dx dy, \quad (4.4)$$

where

$$\widehat{f}_{i+\frac{1}{2},j} = \sum_{\beta} w_{\beta} F \left( U_{x_{i+\frac{1}{2}},y_j^{\beta}}^{-}, U_{x_{i+\frac{1}{2}},y_j^{\beta}}^{+} \right), \quad (4.5)$$

is an approximation to the integration of  $f$  in  $y$ -direction:

$$\frac{1}{\Delta y} \int_{y_{j-\frac{1}{2}}}^{y_{j+\frac{1}{2}}} f(U(x_{i+\frac{1}{2}}, y, t)) dy.$$

$U_{x_{i+\frac{1}{2}},y_j^{\beta}}^{\pm}$  are the high-order pointwise approximations to  $U((x_{i+\frac{1}{2}}, y_j^{\beta}), t)$  by a one-dimensional WENO reconstruction procedure and the Lax-Friedrichs flux

$$F(a_1, a_2) = \frac{1}{2}(f(a_1) + f(a_2) - \alpha_1(a_2 - a_1)), \quad \alpha_1 = \max(|u| + \sqrt{gh}),$$

is used. The other flux  $\widehat{g}_{i,j+\frac{1}{2}}$  is computed in the similar way with

$$G(a_1, a_2) = \frac{1}{2}(g(a_1) + g(a_2) - \alpha_2(a_2 - a_1)), \quad \alpha_2 = \max(|v| + \sqrt{gh}).$$

It is straightforward to extend our well-balanced WENO scheme in Section 2 to two dimensions, and we refer to [38] for the details. Let  $\widehat{f}_{i+\frac{1}{2},j}^l, \widehat{f}_{i-\frac{1}{2},j}^r, \widehat{g}_{i,j+\frac{1}{2}}^l$  and  $\widehat{g}_{i,j-\frac{1}{2}}^r$  be the well-balanced fluxes defined similarly as in (2.6). Then the well-balanced version of the 2D WENO method is

$$\frac{U^{n+1} - U^n}{\Delta t} = -\frac{1}{\Delta x} \left( \widehat{f}_{i+\frac{1}{2},j}^l - \widehat{f}_{i-\frac{1}{2},j}^r \right) - \frac{1}{\Delta y} \left( \widehat{g}_{i,j+\frac{1}{2}}^l - \widehat{g}_{i,j-\frac{1}{2}}^r \right) + s_{i,j}. \quad (4.6)$$

where

$$s_{i,j} \approx \frac{1}{\Delta x \Delta y} \int_{I_{i,j}} s(h, b) dx dy.$$

In the second equation of (4.1), it is equal to

$$\frac{1}{\Delta x} \sum_{\beta} w_{\beta} \left( \int_{I_i} s(h_h, b_h)(x, y_j^{\beta}) dx \right), \quad (4.7)$$

where  $\int_{I_i} s(h_h, b_h)(x, y_j^{\beta}) dx$  is computed in the same fashion as in the one-dimensional case, which is shown at the end of Section 2. This means that at each Gauss point in the  $y$  direction, we interpolate polynomials as functions of  $x$ , and use them to compute the source term. Similarly, we can handle the third equation in (4.1) in the same way.

For the positivity-preserving purpose, we will still need to use the Gauss-Lobatto quadrature rule, and we distinguish it from the Gauss quadrature (4.3) by adding hats to the Gauss-Lobatto points, i.e.,

$$\widehat{S}_i^x = \{\widehat{x}_i^r : r = 1, \dots, N\}, \quad \widehat{S}_j^y = \{\widehat{y}_j^r : r = 1, \dots, N\} \quad (4.8)$$

will denote the Gauss-Lobatto quadrature points on  $[x_{i-\frac{1}{2}}, x_{i+\frac{1}{2}}]$  and  $[y_{j-\frac{1}{2}}, y_{j+\frac{1}{2}}]$ , respectively. Recall from Remark 3.6 that the Gauss-Lobatto quadrature (4.8) is introduced to prove the positivity only, and Gauss quadrature (4.3) is used in (4.5) and (4.7) to compute the integrals. Let  $\widehat{w}_r$  be the Gauss-Lobatto quadrature weights for the interval  $[-1/2, 1/2]$  such that  $\sum_{r=1}^N \widehat{w}_r = 1$ . In the following context, subscripts or superscripts  $\beta$  will be used only for Gauss quadrature points and  $r$  only for Gauss-Lobatto points.

We have

$$\overline{h}_{i,j}^n = \frac{1}{\Delta x \Delta y} \iint_{I_{i,j}} p_{i,j}(x, y) dx dy = \sum_{\beta=1}^L w_{\beta} \sum_{r=1}^N \widehat{w}_r p_{i,j}(x_i^{\beta}, \widehat{y}_j^r) = \sum_{r=1}^N \widehat{w}_r \sum_{\beta=1}^L w_{\beta} p_{i,j}(\widehat{x}_i^r, y_j^{\beta}) \quad (4.9)$$

since the quadrature is exact for polynomials of degree  $2k - 2$ . If we introduce the variables

$$\xi_{i,j}^1 = \sum_{\beta=1}^L w_{\beta} \sum_{r=2}^{N-1} \widehat{w}_r p_{i,j}(x_i^{\beta}, \widehat{y}_j^r) = \frac{\overline{h}_{i,j}^n - \widehat{w}_1 \sum_{\beta=1}^L w_{\beta} p_{i,j}(x_i^{\beta}, y_{j-\frac{1}{2}}) - \widehat{w}_N \sum_{\beta=1}^L w_{\beta} p_{i,j}(x_i^{\beta}, y_{j+\frac{1}{2}})}{1 - \widehat{w}_1 - \widehat{w}_N} \quad (4.10)$$

$$\xi_{i,j}^2 = \sum_{r=2}^{N-1} \widehat{w}_r \sum_{\beta=1}^L w_{\beta} p_{i,j}(\widehat{x}_i^r, y_j^{\beta}) = \frac{\overline{h}_{i,j}^n - \widehat{w}_1 \sum_{\beta=1}^L w_{\beta} p_{i,j}(x_{i-\frac{1}{2}}, y_j^{\beta}) - \widehat{w}_N \sum_{\beta=1}^L w_{\beta} p_{i,j}(x_{i+\frac{1}{2}}, y_j^{\beta})}{1 - \widehat{w}_1 - \widehat{w}_N} \quad (4.11)$$

we have

$$\begin{aligned} \overline{h}_{i,j}^n &= (1 - \widehat{w}_1 - \widehat{w}_N) \xi_{i,j}^1 + \widehat{w}_1 \sum_{\beta=1}^L w_{\beta} p_{i,j}(x_i^{\beta}, y_{j-\frac{1}{2}}) + \widehat{w}_N \sum_{\beta=1}^L w_{\beta} p_{i,j}(x_i^{\beta}, y_{j+\frac{1}{2}}) \\ &= (1 - \widehat{w}_1 - \widehat{w}_N) \xi_{i,j}^2 + \widehat{w}_1 \sum_{\beta=1}^L w_{\beta} p_{i,j}(x_{i-\frac{1}{2}}, y_j^{\beta}) + \widehat{w}_N \sum_{\beta=1}^L w_{\beta} p_{i,j}(x_{i+\frac{1}{2}}, y_j^{\beta}). \end{aligned} \quad (4.12)$$

Following the approaches in showing Proposition 3.2, we have the result:

**Proposition 4.1:** Consider the well-balanced WENO scheme (4.6) solving (4.1). Let  $\xi_{i,j}^1$  and  $\xi_{i,j}^2$  be defined in (4.10) and (4.11) in  $I_{i,j}$ . If  $h_{i,j}^{\pm}(x_i^{\beta}, y_{j \pm \frac{1}{2}})$ ,  $h_{i,j}^{\pm}(x_{i \pm \frac{1}{2}}, y_j^{\beta})$  and  $\xi_{i,j}^1$ ,  $\xi_{i,j}^2$

are all non-negative for all the  $r, i, j$  at time level  $t^n$ , then  $\bar{h}_{i,j}^{n+1} \geq 0$  under the CFL condition

$$\frac{\Delta t}{\Delta x} \| (|u| + \sqrt{gh}) \|_\infty + \frac{\Delta t}{\Delta y} \| (|v| + \sqrt{gh}) \|_\infty \leq \hat{w}_1. \quad (4.13)$$

The proof is straightforward by using Lemma 3.1 and following the same lines as in [41].

The linear scaling limiter can enforce the sufficient conditions in the proposition above:

$$\tilde{U}_{ij}^n(x, y) = \theta \left( U_{ij}^n(x, y) - \bar{U}_{ij}^n \right) + \bar{U}_{ij}^n, \quad \theta = \min \left\{ 1, \frac{\bar{h}_{ij}^n}{\bar{h}_{ij}^n - m_{i,j}} \right\}, \quad (4.14)$$

where

$$m_{i,j} = \min_{(x,y) \in I_{ij}} h_{ij}^n(x, y). \quad (4.15)$$

As mentioned in Section 3, this involves the evaluation of a polynomial minimum, which we would prefer to avoid. In [40] and [39], (4.15) was replaced by

$$m_{i,j} = \min_{(x,y) \in S_{ij}} h_{ij}^n(x, y), \quad S_{ij} = \left\{ (x, y) : x \in S_i^x, y \in \hat{S}_j^y, \text{ or } x \in \hat{S}_i^x, y \in S_j^y \right\}, \quad (4.16)$$

which is very simple for the discontinuous Galerkin method. However, for the finite volume method, this approach involves the extra reconstruction at these points in  $S_{ij}$ , and becomes rather complicated and time-consuming, as shown in [40]. Here, we propose a simpler approach following (3.15) introduced in Section 3. We first separate this limiter into two, one in the  $x$ -direction and one in  $y$ -direction. In  $x$ -direction, we introduce

$$\tilde{h}_{ij}(x_i^\beta, y_{j \pm \frac{1}{2}}) = \theta \left( h_{ij}^n(x_i^\beta, y_{j \pm \frac{1}{2}}) - \bar{U}_{ij}^n \right) + \bar{h}_{ij}^n, \quad \theta = \min \left\{ 1, \frac{\bar{h}_{ij}^n}{\bar{h}_{ij}^n - m_{i,j}} \right\}, \quad (4.17)$$

to compute  $\tilde{h}_{ij}(x_i^\beta, y_{j \pm \frac{1}{2}})$ , where

$$m_{i,j} = \min(h_{ij}^+(x_i^\beta, y_{j-\frac{1}{2}}), h_{ij}^-(x_i^\beta, y_{j+\frac{1}{2}}), \xi_{i,j}^1). \quad (4.18)$$

In  $y$ -direction, we introduce

$$\tilde{h}_{ij}(x_{i \pm \frac{1}{2}}, y_j^\beta) = \theta \left( h_{ij}^n(x_{i \pm \frac{1}{2}}, y_j^\beta) - \bar{U}_{ij}^n \right) + \bar{h}_{ij}^n, \quad \theta = \min \left\{ 1, \frac{\bar{h}_{ij}^n}{\bar{h}_{ij}^n - m_{i,j}} \right\}, \quad (4.19)$$

to compute  $\tilde{h}_{ij}(x_{i \pm \frac{1}{2}}, y_j^\beta)$ , where

$$m_{i,j} = \min(h_{ij}^+(x_{i-\frac{1}{2}}, y_j^\beta), h_{ij}^-(x_{i+\frac{1}{2}}, y_j^\beta), \xi_{i,j}^2). \quad (4.20)$$

Since  $\xi_{i,j}^1$  and  $\xi_{i,j}^2$  can be computed easily, the computation of  $m_{i,j}$  is very simple. Following the proof of Lemma 3.3, we can show that the approach (4.17) and (4.19) inherits the desirable properties of (4.14), i.e., this limiter does not destroy accuracy, and keeps the conservativity of the water height. By the same argument as in Section 3, the positivity-preserving limiter does not destroy the well-balanced property.

Given the cell average  $\bar{U}_{i,j}^n$  in interval  $I_{i,j}$  at time level  $n$  with a non-negative height cell average  $\bar{h}_{i,j}^n \geq 0$ , the algorithm flowchart of our high-order well-balanced positivity-preserving WENO method with Euler forward in time for the shallow water equations is:

- Use WENO reconstruction to evaluate  $U_{x_i^\beta, y_{j-\frac{1}{2}}}^+$ ,  $U_{x_i^\beta, y_{j+\frac{1}{2}}}^-$ ,  $U_{x_{i-\frac{1}{2}}, y_j^\beta}^+$  and  $U_{x_{i+\frac{1}{2}}, y_j^\beta}^-$ , and compute  $\xi_{i,j}^1$ ,  $\xi_{i,j}^2$  from (4.10), (4.11).
- Evaluate  $m_{i,j}$  by (4.18) and use the positivity preserving limiter (4.17) to compute  $\tilde{h}_{x_i^\beta, y_{j-\frac{1}{2}}}^+$  and  $\tilde{h}_{x_i^\beta, y_{j+\frac{1}{2}}}^-$  in the  $x$  direction. Use (4.20) and (4.19) to compute  $\tilde{h}_{x_{i-\frac{1}{2}}, y_j^\beta}^+$  and  $\tilde{h}_{x_{i+\frac{1}{2}}, y_j^\beta}^-$  in the  $y$  direction.
- Compute  $\tilde{U}^{*,+}$  and  $\tilde{U}^{*,-}$  at the cell boundary following (2.8) and use them instead of  $U^+$ ,  $U^-$  in the WENO scheme (4.6) with the CFL condition (4.13).

For TVD high-order time discretizations, we need to perform the algorithm above in each stage for a Runge-Kutta method or in each step for a multistep method.

## 5 Numerical examples

In this section we present numerical results of our positivity-preserving WENO methods for the one- and two-dimensional shallow water equations. Fifth order finite volume WENO schemes are implemented as examples. Time discretization is by the third order TVD Runge-Kutta time discretization (2.4). Unless otherwise specified, the CFL number is taken as 0.08, to satisfy the requirement that  $\lambda\alpha < 1/12$  in Proposition 3.4. The gravitation constant  $g$  is fixed as  $9.812 \text{ m/s}^2$ .

## 5.1 Test for the well-balanced property

We test our proposed WENO schemes on a still water steady state problem with a non-flat bottom and a wet/dry interface, to verify the well-balanced property. The bottom topography is given by the depth function [25, 39]

$$b(x) = \max(0, 0.25 - 5(x - 0.5)^2), \quad 0 \leq x \leq 1, \quad (5.1)$$

and the initial data is the stationary solution except at the dry area

$$h + b = \max(0.2, b), \quad hu = 0.$$

This equilibrium should be exactly preserved with the periodic boundary condition. We compute the solution until  $t = 0.5$  using 200 uniform cells. The computed surface level  $h + b$  and the bottom  $b$  are plotted in Figure 5.1. In order to demonstrate that the still water solution is indeed maintained up to round-off error, we use single- and double-precision to perform the computation, and show the  $L^1$  and  $L^\infty$  errors for the water height  $h$  and the discharge  $hu$  in Table 5.1 with different precisions. We can clearly see that the  $L^1$  and  $L^\infty$  errors are at the level of round-off errors for different precisions, verifying the well-balanced property.

Table 5.1:  $L^1$  and  $L^\infty$  errors for different precisions for the stationary solution in Section 5.1.

precision	$L^1$ error		$L^\infty$ error	
	$h$	$hu$	$h$	$hu$
single	1.95E-07	6.32E-07	6.79E-06	8.88E-06
double	2.48E-13	1.01E-13	8.12E-12	1.35E-12

## 5.2 Accuracy test

The high order accuracy of our proposed schemes will be tested for a smooth solution. Following the setup in [38], we choose the following bottom topography and initial conditions

$$b(x) = \sin^2(\pi x), \quad h(x, 0) = 5 + e^{\cos(2\pi x)}, \quad (hu)(x, 0) = \sin(\cos(2\pi x)),$$

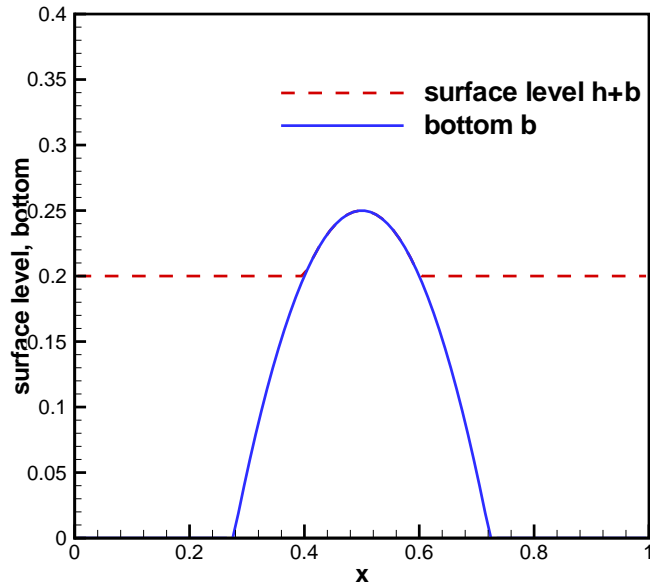


Figure 5.1: The surface level  $h + b$  and the bottom  $b$  for the stationary flow in Section 5.1.

with periodic boundary conditions in the domain  $[0, 1]$ . Since the exact solution is not known explicitly for this case, we use the fifth order finite volume WENO scheme (without the positivity-preserving limiter) from [37] with 12,800 cells to compute a reference solution, and treat this reference solution as the exact solution in computing the numerical errors. We compute up to  $t = 0.1$  when the solution is still smooth (shocks develop later in time for this problem). Table 5.2 contains the  $L^1$  errors for the cell averages and numerical orders of accuracy for the WENO scheme.  $L^\infty$  errors and the corresponding order of accuracy are also provided. Notice that the CFL number we have used for the finite volume scheme decreases with the mesh size and is recorded in Table 5.2. We can clearly see that fifth order accuracy is achieved, which verifies the high order accurate property.

### 5.3 Vacuum occurrence by a double rarefaction wave over a step

This numerical example aims to test the ability of the proposed method to deal with the dry areas over a discontinuous bottom. It was first proposed by Gallouet et al. [19], and also

Table 5.2:  $L^1$  errors and numerical orders of accuracy for the example in Section 5.2.

No. of cells	CFL	$h$		$hu$	
		$L^1$ error	order	$L^1$ error	order
25	0.6	1.71E-02		1.57E-01	
50	0.6	2.78E-03	2.62	2.91E-02	2.43
100	0.4	4.53E-04	2.62	3.84E-03	2.92
200	0.3	3.83E-05	3.56	3.26E-04	3.56
400	0.2	1.66E-06	4.53	1.42E-05	4.52
800	0.1	5.37E-08	4.94	4.63E-07	4.94

appeared in [18, 4].

The channel length is 25, and a discontinuous bottom topography is defined as follows:

$$b(x) = \begin{cases} 1 & \text{if } 25/3 \leq x \leq 12.5, \\ 0 & \text{otherwise.} \end{cases} \quad (5.2)$$

The initial water surface  $h + b$  is set as 10, and the initial discharge is

$$hu(x, 0) = \begin{cases} -350 & \text{if } x \leq 50/3, \\ 350 & \text{otherwise.} \end{cases} \quad (5.3)$$

250 uniform cells are used in the computation. The numerical results at different times  $t = 0, 0.05, 0.25, 0.45$  and  $0.65$  are shown in Figures 5.2 and 5.3 for the water surface and the discharge, respectively. The water flows out of the domain and a dry region is developed. The numerical results reflect this pattern well and agree with those obtained in [19].

## 5.4 Riemann problem over a flat bottom

Two Riemann problems containing dry area over a flat bottom (i.e.  $b(x) \equiv 0$ ) are considered in this subsection, to demonstrate the positivity-preserving ability of our methods. These examples have been used in [8, 39].

The computational domain for the first test case is set as  $[-300, 300]$ , and the initial conditions are given by

$$hu(x, 0) = 0 \quad \text{and} \quad h(x, 0) = \begin{cases} 10 & \text{if } x \leq 0, \\ 0 & \text{otherwise.} \end{cases} \quad (5.4)$$

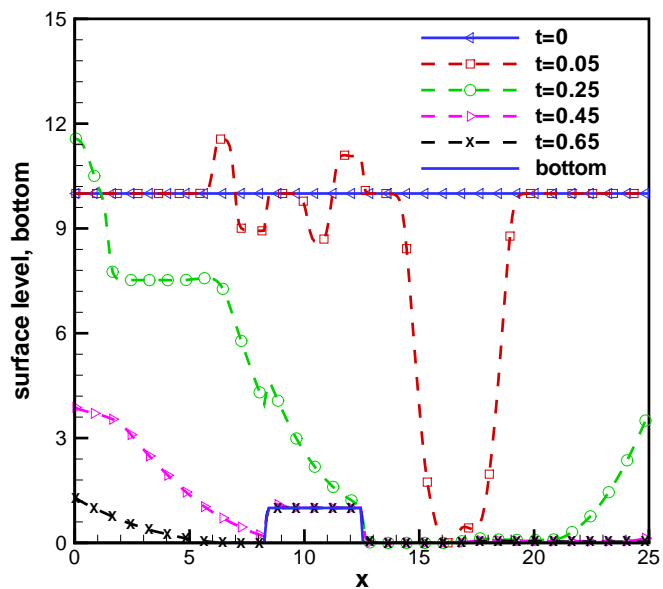


Figure 5.2: Vacuum occurrence by a double rarefaction wave over a step with initial conditions (5.3) and 250 cells. The surface level at different time.

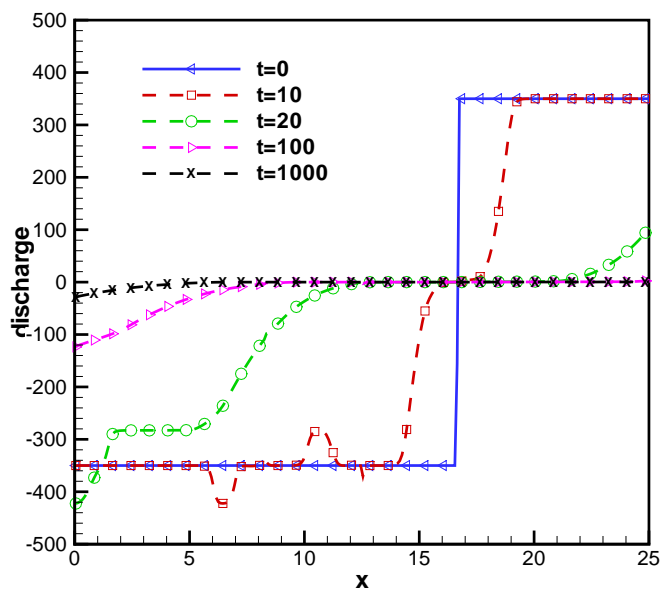


Figure 5.3: Same as in Figure 5.2, the discharge at different time.

The left side is a still water with surface level 10, and the right side is dry region. The analytic solution for this problem can be found in [5]. We compute this problem using our well-balanced positivity-preserving WENO methods with simple transmissive boundary conditions and 250 uniform cells. The solutions at time  $t = 4, 8$  and  $12$  are shown in Figure 5.4. We also plot the exact solutions in these figures to provide a comparison. The zoomed-in version near the wet/dry front at these times is presented in Figure 5.5. From these figures, we observe that the exact solutions are well captured by the numerical results.

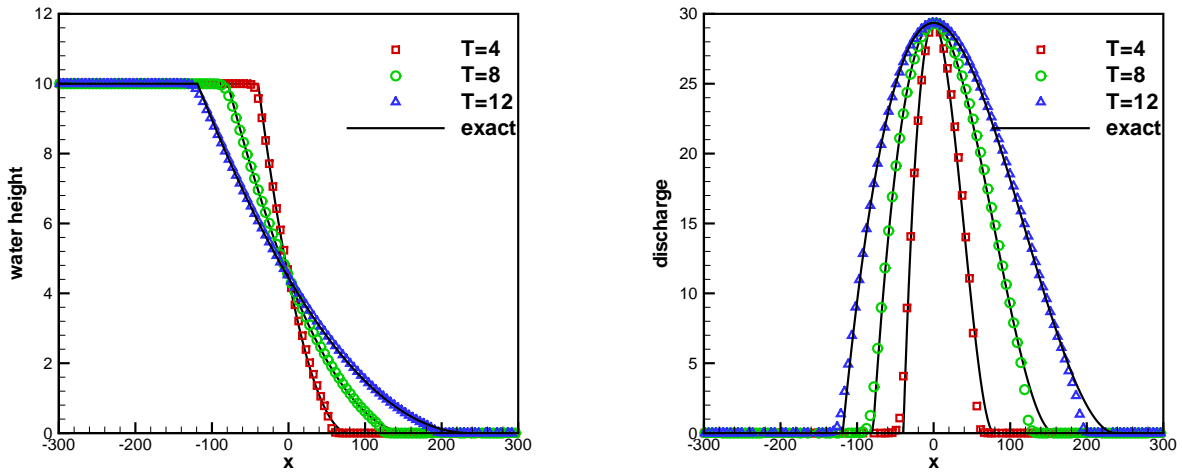


Figure 5.4: The numerical and exact solutions of the first Riemann problem in Section 5.4 at different time with 250 uniform cells. Left: the water height  $h$ ; Right: the discharge  $hu$ .

The second test case is on the computational domain  $[-200, 400]$ . The initial conditions have nonzero velocity, and are given by

$$h(x, 0) = \begin{cases} 5 & \text{if } x \leq 0, \\ 10 & \text{otherwise,} \end{cases} \quad \text{and} \quad u(x, 0) = \begin{cases} 0 & \text{if } x \leq 0, \\ 40 & \text{otherwise,} \end{cases} \quad (5.5)$$

which do not contain dry area. But as the constant initial conditions meet the drying criterion  $\sqrt{gh_l} + \sqrt{gh_r} + u_l - u_r < 0$ , a dry region emerges and this makes the problem numerically difficult. Two expansion waves then propagate away from each other. The analytic solution for this problem can be found in [5]. We compute this problem using our well-balanced positivity-preserving WENO methods with simple transmissive boundary conditions and 250 uniform cells. The numerical solutions, as well as the exact solutions, at

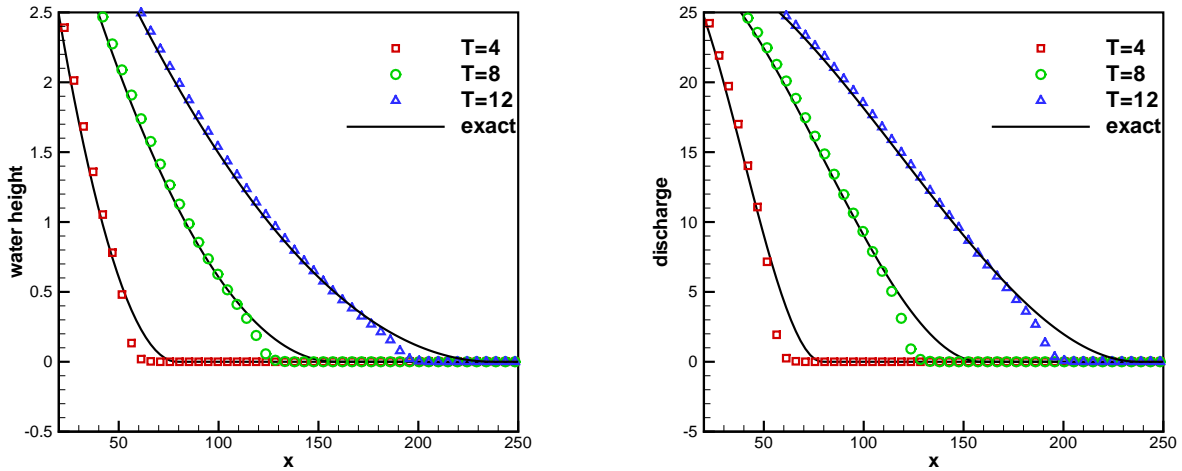


Figure 5.5: Same as in Figure 5.4, zoom-in of the wet/dry front.

time  $t = 2, 4$  and  $6$  are shown in Figure 5.6. We can observe that the numerical solutions agree well with the exact solutions. The comparison near the wet/dry front are shown in Figure 5.7. There exists some observable error near the dry region. We repeat the test with 500 uniform cells and the corresponding solutions are plotted in Figure 5.8, where such error are significantly reduced and a good agreement between the numerical and exact solutions is observed.

We have also run this test case using the well-balanced WENO methods without the positivity-preserving limiter. Negative water height was generated during the computation, which caused blow-up immediately. This confirms the proposed positivity-preserving property of our method.

## 5.5 Parabolic bowl

A test example with a parabolic bottom topography, used in [25] for the shallow water equations with the friction source term, will be considered in this subsection to test the performance of our methods.

The computational domain is set as  $[-5000, 5000]$ . We take the parabolic bottom

$$b(x) = h_0(x/a)^2, \quad (5.6)$$

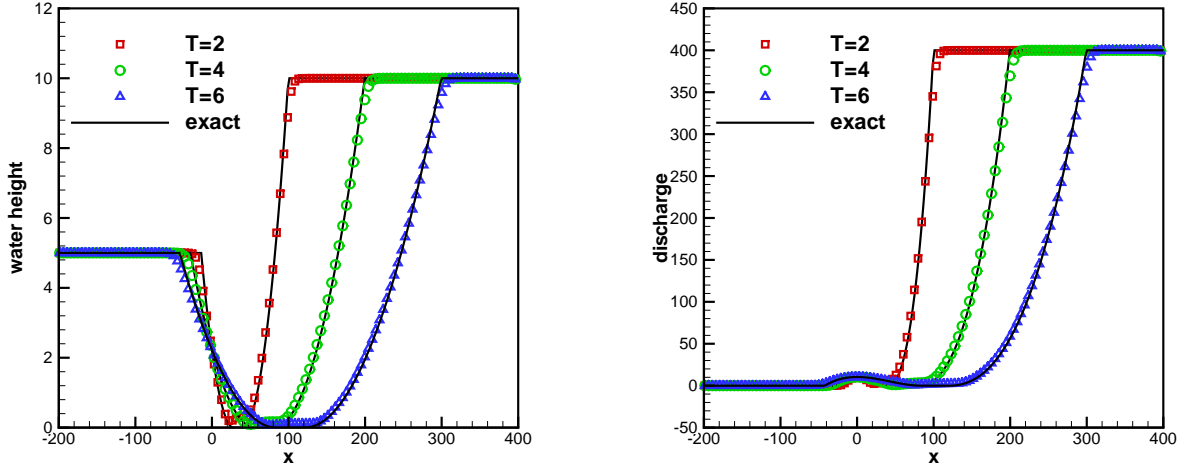


Figure 5.6: The numerical and exact solutions of the second Riemann problem in Section 5.4 at different time with 250 uniform cells. Left: the water height  $h$ ; Right: the discharge  $hu$ .

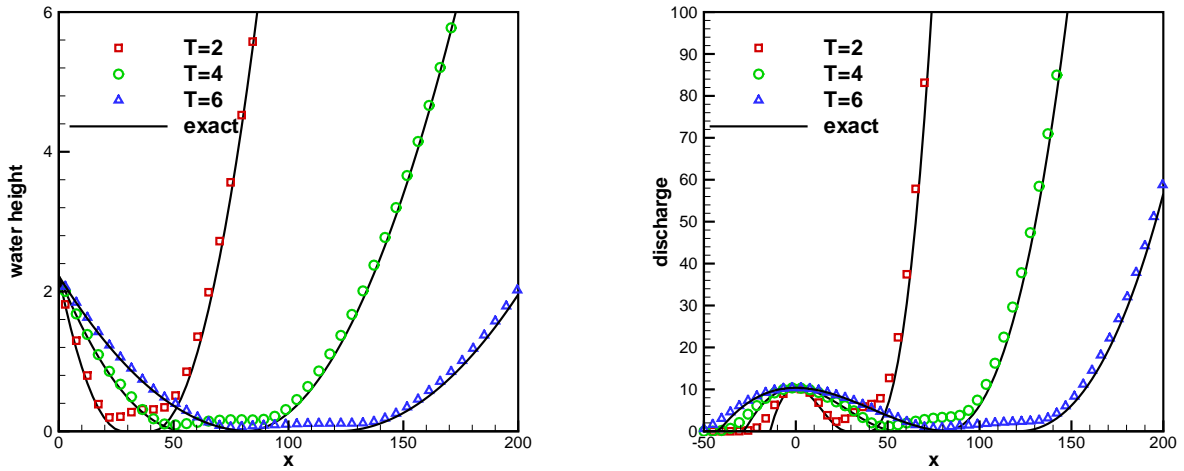


Figure 5.7: Same as in Figure 5.6, zoom-in of the wet/dry front.

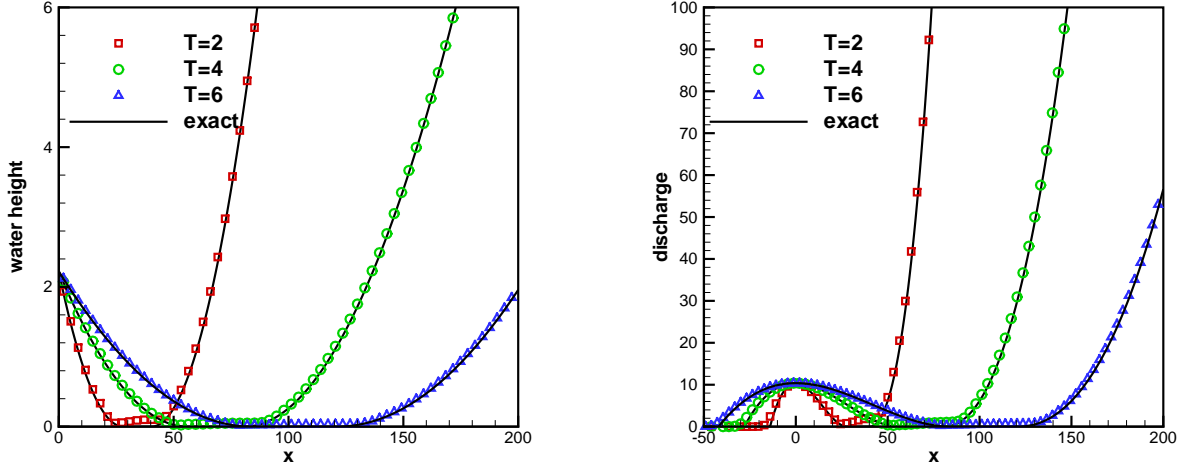


Figure 5.8: Same as in Figure 5.6, zoom-in of the wet/dry front, with 500 uniform cells employed.

with constants  $h_0$  and  $a$  to be specified later. For all one-dimensional shallow water equations with a parabolic bottom topography, analytic solutions have been derived by Sampson et al. [31]. For the bottom (5.6), the analytical water surface for the shallow water equations without the friction source term, is given by

$$h(x, t) + b(x) = h_0 - \frac{B^2}{4g} \cos(2\omega t) - \frac{B^2}{4g} - \frac{Bx}{2a} \sqrt{\frac{8h_0}{g}} \cos(\omega t), \quad (5.7)$$

where  $\omega = \sqrt{2gh_0}/a$  and  $B$  is a given constant. The exact location of the wet/dry front takes the form

$$x_0 = -\frac{B\omega a^2}{2gh_0} \cos(\omega t) \pm a. \quad (5.8)$$

We fix these coefficients to be  $a = 3000$ ,  $B = 5$  and  $h_0 = 10$  for our test case. The initial condition is then given by (5.7) (for the water height) and a zero discharge. Because the flow cannot reach the boundaries, we can pick any boundary conditions and they have no impact on the numerical solutions. We run the simulation until  $T = 6000$  with 250 uniform cells, and plot the numerical water surface at different times in Figure 5.9. We also include the analytical solution to provide a comparison, and a nice agreement can be observed. This confirms the positivity-preserving property of our methods.

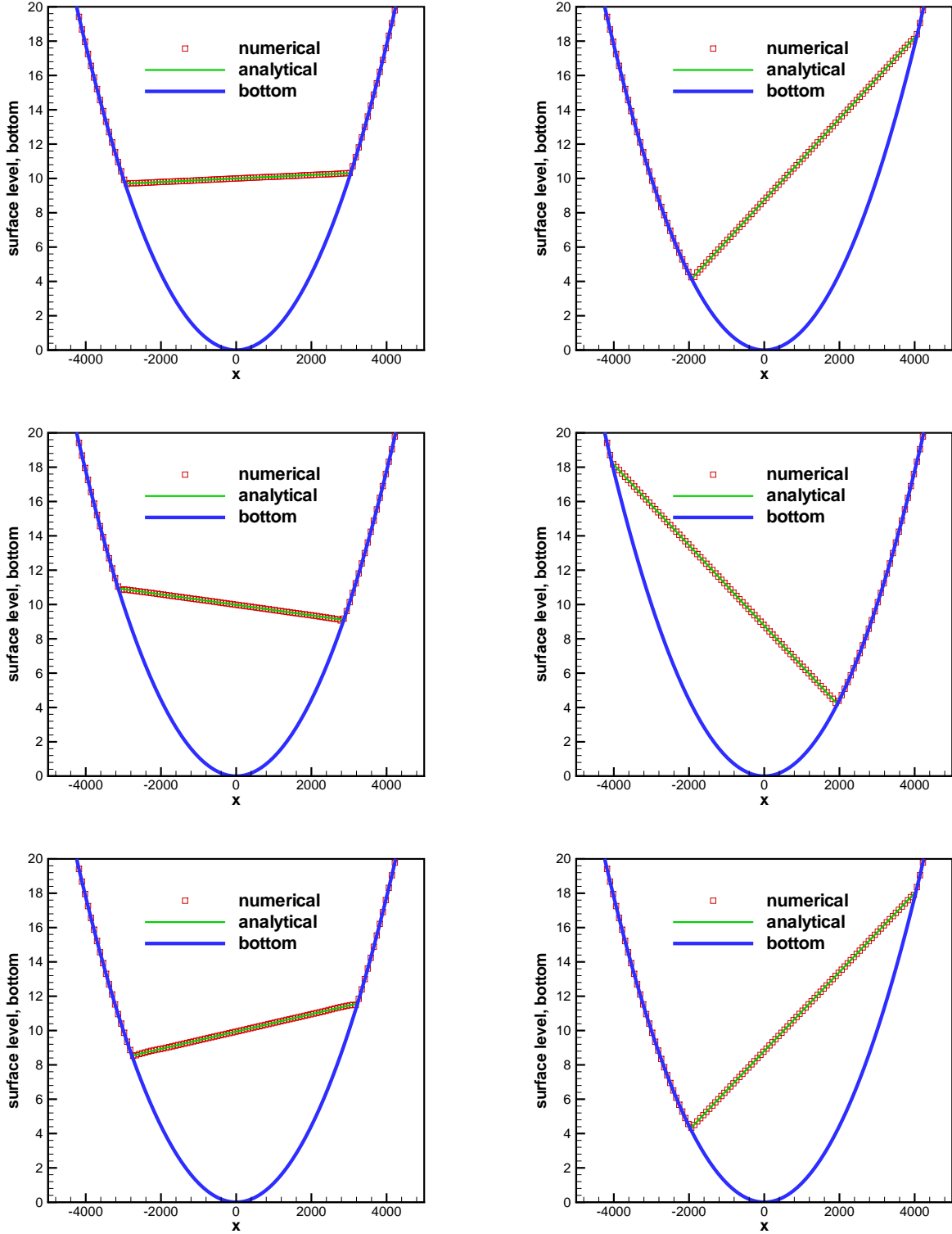


Figure 5.9: The water surface level in the parabolic bowl problem at different time. Top left:  $t = 1000$ ; Top right:  $t = 2000$ ; Middle left:  $t = 3000$ ; Middle right:  $t = 4000$ ; Bottom left:  $t = 5000$ ; Bottom right:  $t = 6000$ .

## 5.6 Oblique 2D dam break

In this two-dimensional test from [4], we consider the evolution of water over a flat bottom, which generates a moving front with an inclination of  $45^\circ$  degree with respect to the boundary of the computational domain.

The initial condition, as illustrated in Figure 5.10, is given by:

$$h(x, y, 0) = \begin{cases} 1 & \text{if } x + y \leq 0, \\ 0 & \text{otherwise,} \end{cases} \quad \text{and} \quad hu(x, y, 0) = hv(x, y, 0) = 0, \quad (5.9)$$

on a square domain  $[-0.5, 0.5] \times [-0.5, 0.5]$ . Still water of height 1 is present in half of the domain and dry area appears in the other half. The analytic solution of this test is available in the literature [5]. Using the transmissive boundary condition and 100 uniform cells in each direction, we solve this problem with the proposed well-balanced positivity-preserving WENO method. The surface elevations on the central cross section (the  $x = y$  plane) orthogonal to the propagating front, are shown in Figure 5.11, at different times  $t = 0, 0.02, 0.06$  and  $0.1$ . The exact solutions are also provided in this figure for comparison. The zoomed-in plot near the propagating front is shown in Figure 5.12. We notice that the numerical solutions match the analytical ones well.

## 6 Concluding remarks

A high-order mass-conserving finite volume WENO method for the shallow water equations with dry areas has been developed in this paper. The proposed method has the properties of being high-order accurate, well-balanced for the still water and preserving the non-negativity of the water height without loss of mass conservation. A positivity-preserving limiter has been introduced, as well as an efficient way to implement it under the WENO framework. This method has been extended to the two-dimensional problem with rectangular meshes. Numerical examples are provided at the end to demonstrate the proposed well-balanced property, accuracy, positivity-preserving property, and non-oscillatory shock resolution of the proposed numerical method. Future work includes the extension to the two-layer shallow

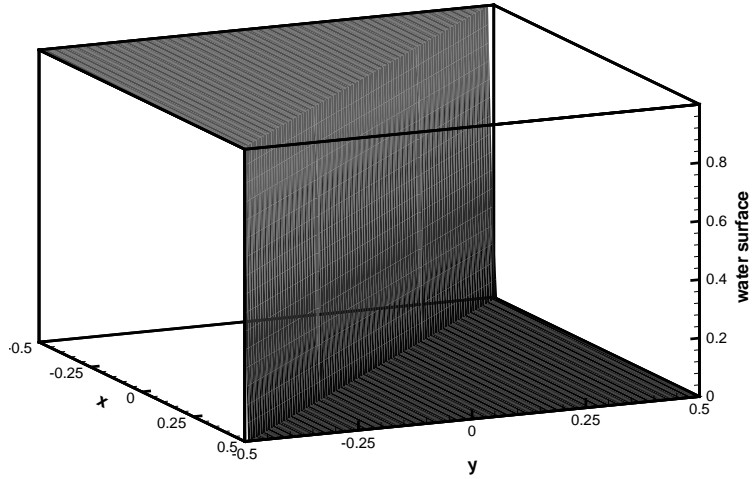


Figure 5.10: Oblique 2D dam break on a dry bed problem. The initial surface level.

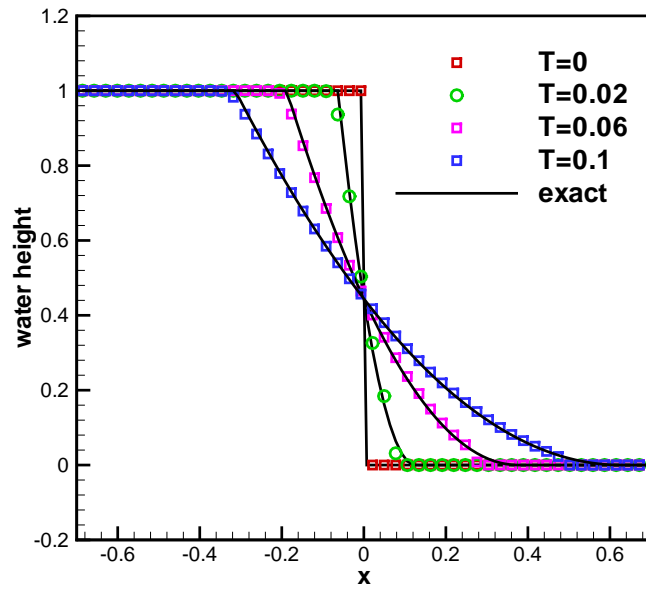


Figure 5.11: Oblique 2D dam break on a dry bed problem. Numerical and analytical surface level at different times in the central cross section.

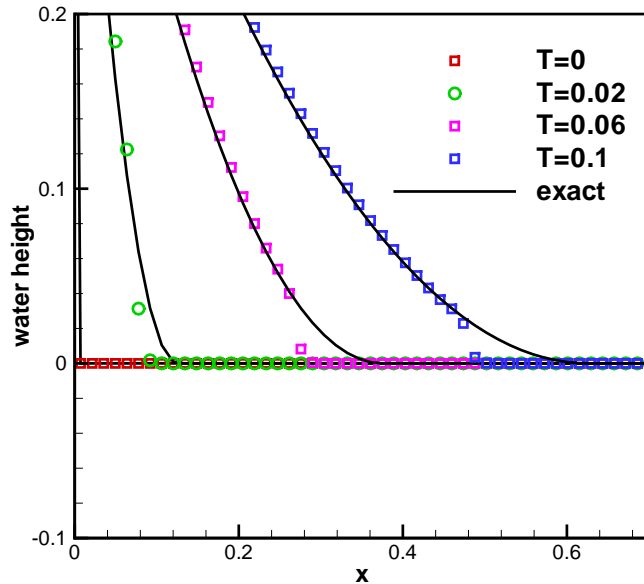


Figure 5.12: Same as in Figure 5.11, zoom-in of the wet/dry front.

water equation and the application to the shallow water model on a rotating sphere.

## References

- [1] E. Audusse, F. Bouchut, M.-O. Bristeau, R. Klein, and B. Perthame. A fast and stable well-balanced scheme with hydrostatic reconstruction for shallow water flows. *SIAM Journal on Scientific Computing*, 25:2050–2065, 2004.
- [2] D. S. Bale, R. J. LeVeque, S. Mitran, and J. A. Rossmannith. A wave propagation method for conservation laws and balance laws with spatially varying flux functions. *SIAM Journal on Scientific Computing*, 24:955–978, 2002.
- [3] A. Bermudez and M. E. Vazquez. Upwind methods for hyperbolic conservation laws with source terms. *Computers and Fluids*, 23:1049–1071, 1994.
- [4] C. Berthon and F. Marche. A positive preserving high order VFRoe scheme for shallow water equations: A class of relaxation schemes. *SIAM Journal on Scientific Computing*, 30:2587–2612, 2008.

- [5] O. Bokhove. Flooding and drying in discontinuous Galerkin finite-element discretizations of shallow-water equations. Part 1: one dimension. *Journal of Scientific Computing*, 22:47–82, 2005.
- [6] A. Bollermann, S. Noelle, and M. Lukáčová-Medviová. Finite volume evolution Galerkin methods for the shallow water equations with dry beds. *Communications in Computational Physics*, in press, 2010.
- [7] P. Brufau, M. E. Vázquez-Cendón, and P. García-Navarro. A numerical model for the flooding and drying of irregular domains. *International Journal for Numerical Methods in Fluids*, 39:247–275, 2002.
- [8] S. Bunya, E. J. Kubatko, J. J. Westerink, and C. Dawson. A wetting and drying treatment for the Runge-Kutta discontinuous Galerkin solution to the shallow water equations. *Computer Methods in Applied Mechanics and Engineering*, 198:1548–1562, 2009.
- [9] V. Caleffi and A. Valiani. Well-balanced bottom discontinuities treatment for high-order shallow water equations WENO scheme. *Journal of Engineering Mechanics*, 135:684–696, 2009.
- [10] V. Caleffi, A. Valiani, and A. Bernini. Fourth-order balanced source term treatment in central WENO schemes for shallow water equations. *Journal of Computational Physics*, 218:228–245, 2006.
- [11] A. Canestrelli, A. Siviglia, M. Dumbser, and E. F. Toro. Well-balanced high-order centred schemes for non-conservative hyperbolic systems. Applications to shallow water equations with fixed and mobile bed. *Advances in Water Resources*, 32:834–844, 2009.
- [12] M. J. Castro, J. M. Gallardo, and C. Parés. High order finite volume schemes based on reconstruction of states for solving hyperbolic systems with nonconservative products.

- Applications to shallow-water systems. *Mathematics of Computation*, 75:1103–1134, 2006.
- [13] M. J. Castro, J. M. González-Vida, and C. Parés. Numerical treatment of wet/dry fronts in shallow flows with a modified Roe scheme. *Mathematical Models and Methods in Applied Sciences*, 16:897–931, 2006.
- [14] C. Dawson and J. Proft. Discontinuous and coupled continuous/discontinuous Galerkin methods for the shallow water equations. *Computer Methods in Applied Mechanics and Engineering*, 191:4721–4746, 2002.
- [15] A. Ern, S. Piperno, and K. Djadel. A well-balanced Runge-Kutta discontinuous Galerkin method for the shallow-water equations with flooding and drying. *International Journal for Numerical Methods in Fluids*, 58:1–25, 2008.
- [16] C. Eskilsson and S. J. Sherwin. A triangular spectral/hp discontinuous Galerkin method for modelling 2D shallow water equations. *International Journal for Numerical Methods in Fluids*, 45:605–623, 2004.
- [17] U. Fjordholm, S. Mishra, and E. Tadmor. Well-balanced and energy stable schemes for the shallow water equations with discontinuous topography. submitted, 2010.
- [18] J. M. Gallardo, C. Parés, and M. Castro. On a well-balanced high-order finite volume scheme for shallow water equations with topography and dry areas. *Journal of Computational Physics*, 227:574–601, 2007.
- [19] T. Gallouët, J.-M. Hérard, and N. Seguin. Some approximate Godunov schemes to compute shallow-water equations with topography. *Computers and Fluids*, 32:479–513, 2003.

- [20] F. X. Giraldo, J. S. Hesthaven, and T. Warburton. Nodal high-order discontinuous Galerkin methods for the spherical shallow water equations. *Journal of Computational Physics*, 181:499–525, 2002.
- [21] G. Jiang and C.-W. Shu. Efficient implementation of weighted ENO schemes. *Journal of Computational Physics*, 126:202–228, 1996.
- [22] S. Jin and X. Wen. Two interface type numerical methods for computing hyperbolic systems with geometrical source terms having concentrations. *SIAM Journal on Scientific Computing*, 26:2079–2101, 2005.
- [23] A. Kurganov and D. Levy. Central-upwind schemes for the Saint-Venant system. *Mathematical Modelling and Numerical Analysis*, 36:397–425, 2002.
- [24] R. J. LeVeque. Balancing source terms and flux gradients on high-resolution Godunov methods: the quasi-steady wave-propagation algorithm. *Journal of Computational Physics*, 146:346–365, 1998.
- [25] Q. Liang and F. Marche. Numerical resolution of well-balanced shallow water equations with complex source terms. *Advances in Water Resources*, 32:873–884, 2009.
- [26] R. Liska and B. Wendroff. Two-dimensional shallow water equations by composite schemes. *International Journal for Numerical Methods in Fluids*, 30:461–479, 1999.
- [27] S. Noelle, N. Pankratz, G. Puppo, and J.R. Natvig. Well-balanced finite volume schemes of arbitrary order of accuracy for shallow water flows. *Journal of Computational Physics*, 213:474–499, 2006.
- [28] C. Parés. Numerical methods for nonconservative hyperbolic systems. A theoretical framework. *SIAM Journal on Numerical Analysis*, 44:300–321, 2006.
- [29] B. Perthame and C.-W. Shu. On positivity preserving finite volume schemes for Euler equations. *Numerische Mathematik*, 273:119–130, 1996.

- [30] B. Perthame and C. Simeoni. A kinetic scheme for the Saint-Venant system with a source term. *Calcolo*, 38:201–231, 2001.
- [31] J. Sampson, A. Easton, and M. Singh. Moving boundary shallow water flow above parabolic bottom topography. *ANZIAM Journal*, 47:C373–378, 2006.
- [32] J. Shi, C. Hu, and C.-W. Shu. A technique of treating negative weights in WENO schemes. *Journal of Computational Physics*, 175:108–127, 2002.
- [33] C.-W. Shu. Total-variation-diminishing time discretizations. *SIAM Journal on Scientific and Statistical Computing*, 9:1073–1084, 1988.
- [34] C.-W. Shu. Essentially non-oscillatory and weighted essentially non-oscillatory schemes for hyperbolic conservation laws. In A. Quarteroni, editor, *Advanced Numerical Approximation of Nonlinear Hyperbolic Equations*, pages 325–432. Lecture Notes in Mathematics, volume 1697, Springer, 1998.
- [35] C.-W. Shu and S. Osher. Efficient implementation of essentially non-oscillatory shock-capturing schemes. *Journal of Computational Physics*, 77:439–471, 1988.
- [36] Y. Xing and C.-W. Shu. High order finite difference WENO schemes with the exact conservation property for the shallow water equations. *Journal of Computational Physics*, 208:206–227, 2005.
- [37] Y. Xing and C.-W. Shu. High order well-balanced finite volume WENO schemes and discontinuous Galerkin methods for a class of hyperbolic systems with source terms. *Journal of Computational Physics*, 214:567–598, 2006.
- [38] Y. Xing and C.-W. Shu. A new approach of high order well-balanced finite volume WENO schemes and discontinuous Galerkin methods for a class of hyperbolic systems with source terms. *Communications in Computational Physics*, 1:100–134, 2006.

- [39] Y. Xing, X. Zhang, and C.-W. Shu. Positivity-preserving high order well-balanced discontinuous Galerkin methods for the shallow water equations. *Advances in Water Resources*, 33, 2010.
- [40] X. Zhang and C.-W. Shu. On maximum-principle-satisfying high order schemes for scalar conservation laws. *Journal of Computational Physics*, 229:3091–3120, 2010.
- [41] X. Zhang and C.-W. Shu. On positivity preserving high order discontinuous galerkin schemes for compressible euler equations on rectangular meshes. *Journal of Computational Physics*, 229:8918–8934, 2010.
- [42] X. Zhang and C.-W. Shu. Maximum-principle-satisfying and positivity-preserving high order schemes for conservation laws: Survey and new developments. *Proceedings of the Royal Society A*, submitted, 2011.